



# Identification of two lipid phosphatases that regulate sphingosine-1-phosphate cellular uptake and recycling

Mari Kono<sup>1</sup>, Lila E. Hoachlander-Hobby<sup>1</sup>, Saurav Majumder<sup>1</sup>, Ronit Schwartz<sup>1</sup>, Colleen Byrnes, Hongling Zhu<sup>1</sup>, and Richard L. Proia<sup>1\*</sup>

Genetics of Development and Disease Section, Genetics and Biochemistry Branch, National Institute of Diabetes and Digestive and Kidney Diseases, National Institutes of Health, Bethesda MD, USA

**Abstract** Sphingosine-1-phosphate (SIP) is a sphingolipid metabolite that serves as a potent extracellular signaling molecule. Metabolic regulation of extracellular SIP levels impacts key cellular activities through altered SIP receptor signaling. Although the pathway through which SIP is degraded within the cell and thereby eliminated from reuse has been previously described, the mechanism used for SIP cellular uptake and the subsequent recycling of its sphingoid base into the sphingolipid synthesis pathway is not completely understood. To identify the genes within this SIP uptake and recycling pathway, we performed a genome-wide CRISPR/Cas9 KO screen using a positive-selection scheme with Shiga toxin, which binds a cell-surface glycosphingolipid receptor, globotriaosylceramide (Gb3), and causes lethality upon internalization. The screen was performed in HeLa cells with their sphingolipid de novo pathway disabled so that Gb3 cell-surface expression was dependent on salvage of the sphingoid base of SIP taken up from the medium. The screen identified a suite of genes necessary for SIP uptake and the recycling of its sphingoid base to synthesize Gb3, including two lipid phosphatases, *PLPP3* (phospholipid phosphatase 3) and *SGPPI* (SIP phosphatase 1). The results delineate a pathway in which plasma membrane-bound PLPP3 dephosphorylates extracellular SIP to sphingosine, which then enters cells and is rephosphorylated to SIP by the sphingosine kinases. This rephosphorylation step is important to regenerate intracellular SIP as a branch-point substrate that can be routed either for dephosphorylation to salvage sphingosine for recycling into complex sphingolipid synthesis or for degradation to remove it from the sphingolipid synthesis pathway.

**Supplementary Key words** Sphingolipids • Sphingosine phosphate • Lysophospholipid • Ceramides • CRISPR/Cas9

Sphingolipids, a major lipid class in eukaryotic cells, are characterized by a sphingoid base backbone, often 18-carbon sphingosine. Their biosynthesis occurs through de novo synthesis and via sphingoid base

salvage and recycling into the sphingolipid synthesis pathway (1–3). De novo sphingolipid synthesis takes place in the endoplasmic reticulum (ER) and is initiated by serine palmitoyltransferase. Subsequent enzyme reactions in the ER produce ceramide, composed of a sphingoid base and a fatty acid. Ceramide is modified to generate plasma membrane sphingolipids—sphingomyelin and glycosphingolipids—by the addition of hydrophilic head groups. In the salvage process, sphingoid bases derived from sphingolipids are recycled for the synthesis of ceramide.

Sphingosine-1-phosphate (SIP) is a bioactive sphingolipid metabolite that is transported into the circulation and regulates key physiological functions through interactions with five G protein-coupled receptors (4, 5). Changes in sphingolipid metabolic enzymes and transporters that modify extracellular SIP levels have dramatic physiological effects due to altered SIP receptor signaling (6–8). The rapid clearance of SIP from blood in vivo suggests that cellular-uptake mechanisms regulate its levels (9–11). Indeed, a blood SIP clearance pathway mediated by hepatocytes has been described, which leads to its degradation by SIP lyase to form phosphoethanolamine and a long-chain aldehyde and subsequently results in its removal from the sphingolipid synthesis pathway (12). However, the other possible metabolic fate of SIP taken up by cells—sphingoid base salvage for ceramide and complex sphingolipid synthesis—has not been clearly delineated. Here, we use a genome-wide clustered regularly interspersed short palindromic repeats (CRISPR)/Cas9 KO screen in HeLa cells to identify the genes that populate this pathway.

## MATERIALS AND METHODS

### Reagents

Antibodies and cell lines used are listed in [supplemental Table S1](#). Four-well chamber plates ( $\mu$ -slide 4 well, 80426) were obtained from Ibidi (Gräfelfing, Germany). Hygromycin B, puromycin, blasticidin, G418, and Lipofectamine 3000 reagent were purchased from Thermo Fisher Scientific

\*For correspondence: Richard L. Proia, [proia@nih.gov](mailto:proia@nih.gov).



(Waltham, MA). Human genome-wide CRISPR/Cas9 KO (GeCKOv2) CRISPR KO pooled library was a gift from Feng Zhang (Addgene, Watertown, MA; Cat# 1000000049), and the lentiviral packaging of the library was accomplished by Vector Builder (Chicago, IL). SIP was purchased from Avanti Polar Lipids (Alabaster, AL), Shiga toxin 2 from *Escherichia coli* was obtained from List Labs (Campbell, CA), and myriocin was obtained from Cayman Chemical (Ann Arbor, MI).

### Genome-wide CRISPR/Cas9 KO library screening and single guide RNA sequence analysis

HeLa cells stably expressing Cas9 (referred as WT HeLa cells in results and figures) were transfected with the pGS-single guide RNA (sgRNA)-Neo plasmid containing the sgRNA sequence of *SPTLC1* (supplemental Table S2) using Lipofectamine 3000 reagent and selected with G418 (400 µg/ml) to disrupt the *SPTLC1* gene. The *SPTLC1* KO HeLa cells expressing Cas9 ( $9.3 \times 10^7$ , referred as *SPTLC1* KO HeLa cells in results and figures), were transduced with the human GeCKO v2 libraries (13) to achieve a total coverage of ~50x with a multiplicity of infection (MOI) of 0.25. Puromycin (1 µg/ml) was added 48 h after transduction. Five days after puromycin selection, one-third of the cells were frozen as input, and two-thirds of the cells were replated with 2 µM of SIP, dissolved in DMSO, added to the culture medium. The next day, one half of the cells were exposed to 2.5 ng/ml Shiga toxin for 15 days in culture. After the SIP and toxin treatment, the cells were harvested and the genomic DNA was isolated using a QIAGEN Blood & Cell Culture DNA Maxi kit (Germantown, MD) according to the manufacturer's protocol. Genomic DNA (400 µg) from each group was used as template DNA to amplify the sgRNA region by PCR. Separate PCR reactions (80 × 100 µl) with 5 µg genomic DNA were set up using NEBNext Ultra TM II Q5 master mix (New England Biolabs, Ipswich, MA; Cat# M0544L) with the following primer set: forward 5'- AATGGACTATCATATGCTTACCGTAACCTTGAAAGTATTTCCG -3'; reverse: 5'-CTTTAGTTTGTATGTCTGT TGCTATTATGTCTACTATTCTTTCCA -3'. All PCR reactions were combined and 150 µl of the combined reaction solution was purified with a Zymo-Spin V column (Zymo Research, Irvine, CA) and eluted with 150 µl of the elution buffer. A second-round PCR reaction was performed (13 × 100 µl) using the purified PCR product (10 µl) to amplify and attach Illumina compatible multiplexing sequencing adapters. Finally, PCR products were purified by gel extraction and quantified by Kapa Library Quantification qPCR (Roche, Basel, Switzerland). The libraries were subjected to single-end sequencing by Illumina NextSeq (San Diego, CA) for input, control (+SIP/-Shiga toxin), and treated (+SIP/+Shiga toxin) cells to identify the copy number of sgRNAs. Sequence reads were analyzed using the Mageck Model-based Analysis of Genome-wide CRISPR-Cas9 KO (MAGeCK) computational tool (14). The resultant scores were presented in figures by R script.

### Generation of knockdown HeLa cell lines

pLentiGuide-plasmids containing sgRNA sequences of *SGPPI*, *PLPP3* (*PPAP2B*), *SPHK1*, *SPHK2*, or *SGPL1* (supplemental Table S2) were used for lentiviral production. The lentivirus packaging was performed by Lenti-X packaging single shots (96-well, VSV-G) and the virus was concentrated using Lenti-X Concentrator according to the manufacturer's instructions (Takara Bio USA, San Jose, CA). HeLa cells stably expressing Cas9 ( $3 \times 10^5$ ) were transduced

with lentivirus at an MOI of 10 and replated 24 h after transduction into T75 flasks. Puromycin (1 µg/ml) or blasticidin (10 µg/ml) was added 48 h after transduction. After three weeks of antibiotic selection, the loci targeted by sgRNAs were evaluated by DNA sequencing. Protein expression levels in knockdown (KD) cells were validated by Western blot except for *SGPPI* KD cells as there was no specific detection of *SGPPI* protein. *SGPPI* KD cells were validated by qPCR using TaqMan gene expression assay for *SGPPI* and *ACTB* as a control (supplemental Table S1) on a Quant Studio 3 (Thermo Fisher Scientific).

Based on Western blot, *SPHK1* and *SGPL1* KD pools had negligible protein expression and were used for further experiments. For *PLPP3*, *SPHK2*, *SGPPI* KD, and *SPHK1/2* double knockdown (DKD) cell pools, equivalent protein levels were observed between WT and KD cells, therefore, these cells were sorted into 96-well-plates using a BD FACSAria™ III flow cytometer (BD Biosciences, San Jose, CA) for isolation of individual single cell clones. For *SPHK1/2*, *SPTLC1* triple knockdown (TKD) cells, the pGS-sgRNA-Neo plasmid containing the sgRNA sequence of *SPTLC1* (supplemental Table S2) was transfected to a *SPHK1/2* DKD line using the Lipofectamine 3000 reagent, and individual clones were isolated by cloning cylinders.

### Cell culture

For subcellular localization experiment, nongenetically modified HeLa cells were used. These cells were cultured in DMEM containing 10% FBS and penicillin/streptomycin (100 U/ml). For all other experiments, hygromycin B (250 µg/ml) was supplemented for HeLa cells stably expressing Cas9. KD cells were selected and cultured using the antibiotics listed in supplemental Table S2.

### Western blot analysis

Protein extracts were prepared from WT and KD HeLa cells using RIPA Lysis and Extraction Buffer (Thermo Fisher Scientific) following the manufacturer's protocol. Equal amounts of protein (30 µg) were separated on a NuPAGE Novex 4%–12% Bis-Tris gel (Thermo Fisher Scientific) and transferred onto nitrocellulose membranes using the iBlot2 Blotting System (Thermo Fisher Scientific). Membranes were blocked in 5% nonfat dry milk for 1 h at room temperature and incubated overnight at 4°C with antibodies listed in supplemental Table S1. Membranes were then washed in 5% nonfat dry milk and incubated with the appropriate horseradish peroxidase-conjugated secondary antibody (Millipore, Burlington, MA) in 5% nonfat dry milk. Membranes were detected using the ECL prime Western blotting system (Cytiva, Marlborough, MA) and imaged on the Amersham Imager 680 (GE Healthcare Life Sciences, Marlborough, MA). All blots were probed with β-actin (Abcam, Cambridge, UK) as a loading control. The blots were analyzed using the ImageQuant TL 8.2 image software (GE Healthcare Life Sciences).

### Measurement of globotriaosylceramide synthesis from SIP uptake and recycling

*SPTLC1* KO HeLa cells, *SGPPI*, *PLPP3* (*PPAP2B*), *SPHK1*, *SPHK2*, or *SGPL1* KD HeLa cells were cultured with myriocin (2.5 µM, 0.1% dimethylsulfoxide (DMSO)) for 7 days to inhibit de novo sphingolipid synthesis. Cells were harvested after SIP (3 µM, 0.6% DMSO) treatment for 1, 3, 5 h. For controls, HeLa cells stably expressing Cas9 were used. In some experiments,

SIP was bound to carrier proteins, HDL (Lee Biosolutions, Maryland Heights, MO) (15), and fatty acid-free BSA (Sigma, St. Louis, MO) (16) and exposed to *SPTLC1* KO HeLa cells and control cells for 5h. Cell-surface globotriaosylceramide (Gb3) expression was measured by flow cytometry. Cells were stained with purified anti-CD77 (Gb3) antibody (clone 5B5, BioLegend, San Diego, CA) and labeled with secondary antibody phycoerythrin-conjugated goat anti-mouse IgM (heavy chain) (supplemental Table S1). Cell-surface CD77 expression was analyzed using a BD FACSAria™ III flow cytometer and FlowJo software (FlowJo LLC, Ashland, OR).

### Subcellular localization of SGPP1, PLPP3, SPHK1, SPHK2, and SGPL1

HeLa cells were transfected either with pReceiver-M29 plasmids containing *eGFP-SGPP1*, *eGFP-SPHK1*, or *eGFP-SPHK2*, or with pReceiver-M03 plasmids containing *PLPP3 (PPAP2B)-eGFP* or *SGPL1-eGFP* (GeneCopoeia, Rockville, MD) using the Lipofectamine 3000 reagent. The mCherry2-C1 plasmid was simultaneously transfected to label cytosol. CellLight reagents were added according to the manufacturer's instruction to label organelles 48 h after transfection. NucBlue Live Cell Stain Ready Probe Reagent was added per the manufacturer's instruction prior to confocal microscopy for nuclear staining. The plasmids and organelle markers are listed in supplemental Table S1. The images were captured three days after transfection with a Zeiss confocal microscope (Jena, Germany, LSM710) and were analyzed for colocalization of fluorescent markers using ZEN 2012 SP5 software (Zeiss, Jena, Germany).

### Statistical analyses

GraphPad Prism (v.9, GraphPad Software, San Diego, CA) was used for graphing and statistical analyses with one-way ANOVA and unpaired t-tests. All data are presented as mean ± SD.  $P < 0.05$  was considered to be statistically significant and the  $P$  values are indicated by asterisks in the figures.

## RESULTS

### Development of assay system for monitoring SIP cellular uptake and recycling into the sphingolipid synthesis pathway

We devised a cellular assay based on the expression of a plasma membrane glycosphingolipid to monitor SIP cellular uptake and the salvage of its sphingoid base for recycling into the sphingolipid synthesis pathway. WT HeLa cells express Gb3, a glycosphingolipid that serves as a receptor for Shiga toxin, on their cell-surface (Fig. 1A [top], B and C) and are thus highly susceptible to Shiga toxin-induced cell death due to toxin uptake and subsequent protein-synthesis inhibition (17–19). We have previously shown that disabling de novo sphingolipid synthesis in HeLa cells through the KO of *SPTLC1*, a gene encoding an essential subunit for serine palmitoyltransferase, significantly reduced Gb3 expression (Fig. 1A [middle], B–D) and resulted in Shiga-toxin resistance (20). When the medium of *SPTLC1* KO HeLa cells was supplemented with SIP, Gb3 cell-surface expression was restored to levels equivalent to those of

WT HeLa cells (Fig. 1A [bottom], B and C), indicating that the sphingoid base of SIP was salvaged and recycled into the sphingolipid synthesis pathway under these conditions. The effectiveness of unbound SIP was similar to that of SIP bound to carrier proteins HDL and BSA for the stimulation of Gb3 cell-surface expression (supplemental Fig. S1).

### Genome-wide CRISPR/Cas9 KO screening identifies regulators of SIP cellular uptake and recycling into the sphingolipid synthesis pathway

The SIP-mediated expression of Gb3 on the cell surface of *SPTLC1* KO HeLa cells allowed us to undertake a genome-wide CRISPR/Cas9 KO screen to identify the genes required for SIP cellular uptake and incorporation into the sphingolipid synthesis pathway (Fig. 2A). The screen was based on the ability of Shiga toxin to kill *SPTLC1* KO HeLa-Cas9 cells that express cell-surface Gb3 after exposure to SIP-supplemented medium (Fig. 1A [bottom]). We used a lentivirus-based genome-wide CRISPR/Cas9 KO (GeCKO v2) library containing 123,411 sgRNAs that target 19,050 human genes with generally six sgRNAs per gene (13). After transduction of *SPTLC1* KO HeLa cells expressing Cas9 with the library at an MOI of 0.25, puromycin was used to select for cells that were successfully transduced with an sgRNA-containing lentivirus. The surviving cells were then grown in media containing SIP to induce Gb3 cell-surface expression and treated either with or without Shiga toxin. After a period of cell growth, the genomic DNA of cells in each group was subjected to deep sequencing to identify the sgRNAs.

Relative abundance of sgRNAs present in cells treated with or without Shiga toxin was compared using the MAGeCK algorithm (14). The genes represented by individual sgRNAs were ranked using the modified robust ranking aggregation score from MAGeCK analysis (Fig. 2B and supplemental Table S3). The 10 top-ranked genes included *A4GALT* (Gb3 synthase), *B4GALT5* (lactosylceramide synthase), *UGCG* (glucosylceramide synthase), and *CERS2* (ceramide synthase 2). Each of these genes is directly involved in the Gb3 synthesis pathway, starting with the formation of ceramide (Fig. 2C). The top 20 genes also included presumptive positive regulators of Gb3 expression, including *LAPTM4A* (lysosomal protein transmembrane 4 alpha), *TM9SF2* (transmembrane 9 superfamily member 2), *SLC35A2* (solute carrier family 35 member A2), *TMEM165* (transmembrane protein 165), *GOLPH3* (Golgi phosphoprotein 3), and *AHR* (Aryl hydrocarbon receptor) (Fig. 2B and supplemental Table S3). *LAPTM4A* interacts with Gb3 synthase and activates the enzyme's activity (21, 22). *TM9SF2* is a regulatory factor of endosomal trafficking and Golgi matrix assembly (21, 22). *SLC35A2* transports UDP-galactose into the Golgi for glycosylation (24, 25). *TMEM165*, which is required for glycosylation in Golgi, is a transporter of  $Ca^{2+}$  and  $Mn^{2+}$  (26, 27). *GOLPH3* mediates the

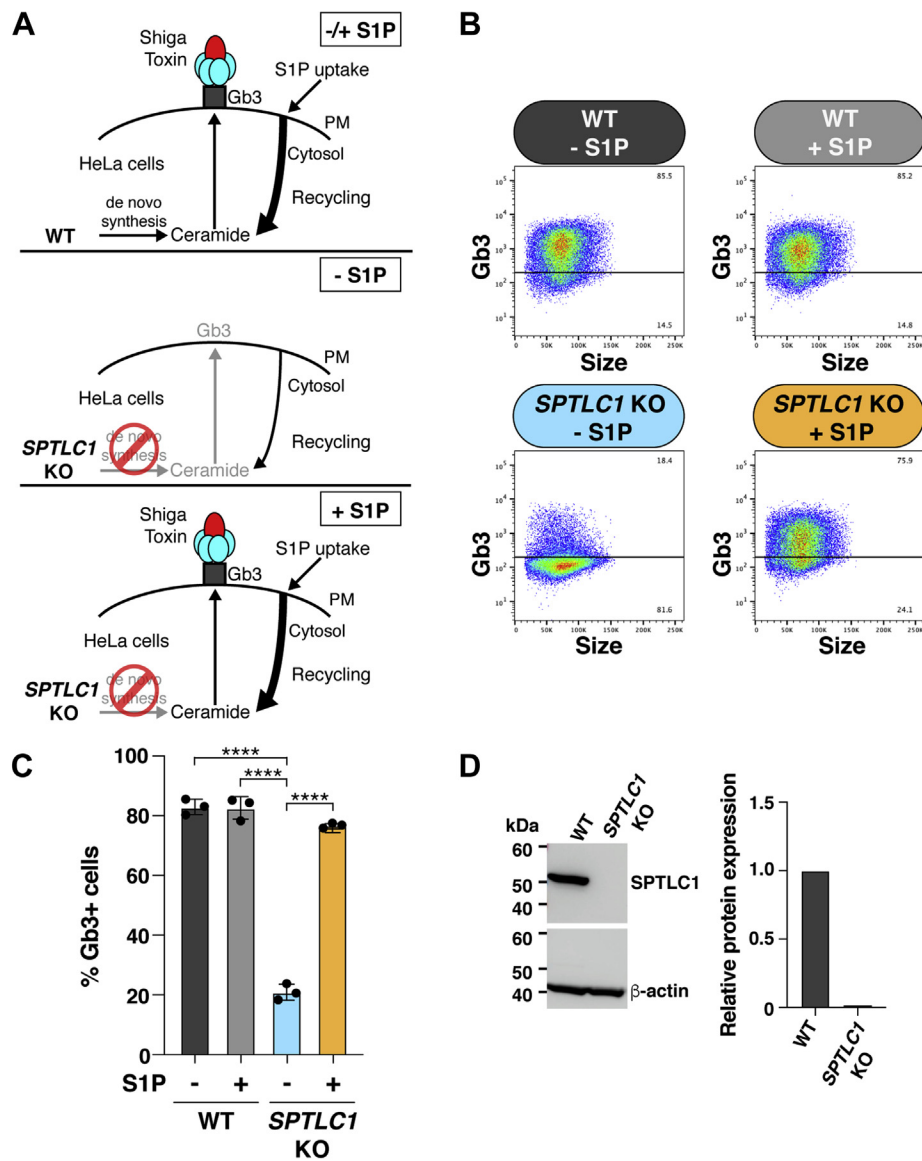


**Fig. 1.** Assay system for monitoring SIP cellular uptake and recycling into the sphingolipid synthesis pathway. **A:** Schematic of experimental design. *Top row*, WT HeLa cells express Shiga toxin receptor, Gb3, on their cell surface regardless of exogenous supplementation with SIP. *Middle row*, *SPTLC1* KO HeLa cells express low levels of cell-surface Gb3. *Bottom row*, supplementation with exogenous SIP restores Gb3 cell-surface expression in *SPTLC1* KO HeLa cells to WT levels. **B:** Flow cytometry analysis of Gb3 cell-surface expression in WT HeLa cells without SIP treatment and after 16 h of 2  $\mu$ M SIP treatment. *Bottom row*, representative dot plots of Gb3 cell-surface expression in *SPTLC1* KO HeLa cells without SIP treatment and after 16 h of 2  $\mu$ M SIP treatment. **C:** Bar graph represents quantification of Gb3 cell-surface expression in WT HeLa and *SPTLC1* KO HeLa cells determined by flow cytometry. Data represent the mean  $\pm$  SD ( $n = 3$ ).  $P$  values were determined by one-way ANOVA followed by Bonferroni's multiple comparisons test; \*\*\*\* $P < 0.0001$ . **D:** Representative Western blot of SPTLC1 protein expression in WT HeLa and *SPTLC1* KO HeLa cells.  $\beta$ -actin was used as a loading control. Bar graph presents quantification of relative SPTLC1 protein expression normalized to  $\beta$ -actin. SPTLC1 protein expression in WT HeLa cells is shown as 1.0. Gb3, globotriaosylceramide; PM, plasma membrane; SIP, sphingosine-1-phosphate.

retention of sphingolipid glycosyltransferases in the Golgi dictating their abundance (28). AHR is a transcription factor that elevates gene expression of the sphingolipid biosynthetic pathway (20).

The top 10 hits also included two lipid phosphatases, *SGPP1* and *PLPP3* (*PPAP2B*) (Fig. 2B, C and supplemental Table S3). *SGPP1* is a SIP-specific phosphatase, and *PLPP3* is a general phospholipid phosphatase that also acts on SIP. These two genes were not previously

identified in Shiga toxin-based screens in cells with the de novo sphingolipid synthesis pathway intact, suggesting that they were specific for the SIP uptake and recycling pathway (20–23).

#### ***PLPP3* or *SGPP1* disruption reduces SIP-stimulated Gb3 cell-surface expression**

To verify that *PLPP3* and *SGPP1* regulate Gb3 cell-surface expression after SIP uptake, we produced

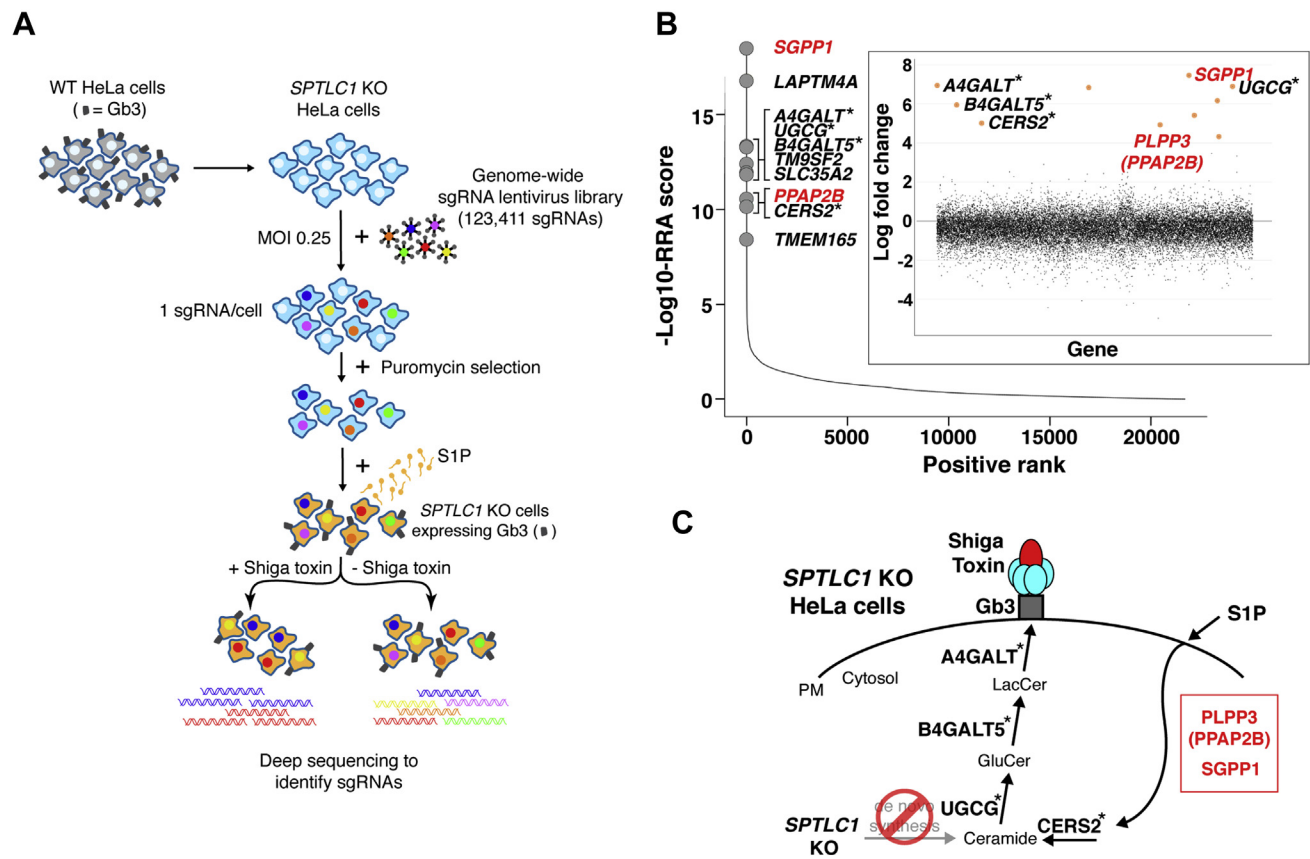


**Fig. 2.** Genome-wide CRISPR/Cas9 KO screen identifies regulators of SIP cellular uptake and recycling into the sphingolipid synthesis pathway. **A:** Schematic of the genome-wide CRISPR/Cas9 KO screening strategy undertaken to identify genes required for SIP uptake and recycling. WT Cas9-expressing HeLa cells (gray); *SPTLC1* KO Cas9-expressing HeLa cells (light blue). Cells were transduced (MOI of 0.25) with a lentivirus-based genome-wide CRISPR/Cas9 KO library and selected in puromycin to yield cells that each contained approximately one viral genome. Cells were grown in media containing SIP (orange) to induce Gb3 cell-surface expression and treated either with or without Shiga toxin. The genomic DNA of cells from each group was subjected to deep sequencing to identify the sgRNAs. **B:** Scatterplot showing the ranking of genes from MAGeCK analysis. X-axis indicates positive ranking of individual genes, and y-axis indicates  $-\text{Log}_{10}$  values of corresponding robust ranking aggregation (RRA) score. The 10 top-ranking genes are highlighted and labeled. *Inset panel*, scatterplot showing log-fold change for all genes. The genes for enzymes directly involved in Gb3 synthesis are marked with asterisks. The genes shown in red are involved in the SIP uptake and recycling pathway. **C:** Schematic showing sphingolipid synthesis pathway leading to the production of Gb3 in *SPTLC1* KO HeLa cells. Top-ranking genes from the screen that are directly involved in Gb3 synthesis are marked with asterisks. *PLPP3* (*PPAP2B*) and *SGPPI*, which are not involved in de novo synthesis of Gb3 (20–23), are involved in the SIP uptake and recycling pathway. CRISPR, clustered regularly interspersed short palindromic repeats; Gb3, globotriaosylceramide; MAGeCK, Model-based Analysis of Genome-wide CRISPR-Cas9 KO; MOI, multiplicity of infection; PM, plasma membrane; SIP, sphingosine-1-phosphate; sgRNA, single guide RNA.

*PLPP3* and *SGPPI* KD HeLa cell lines via Cas9-mediated gene disruption (supplemental Fig. S2A, B). Cells were treated with myriocin for 7 days to inhibit de novo sphingolipid synthesis (Fig. 3A, B), allowing Gb3 synthesis to be limited only to that which could be produced from SIP uptake and sphingoid base salvage. Without myriocin treatment, ~90% of WT HeLa cells expressed Gb3 on their cell surface; myriocin treatment significantly reduced Gb3 cell-surface expression (Fig. 3C). When cells were then exposed to SIP for 1, 3, or 5 h and Gb3 cell-surface expression quantified, *PLPP3* KD cells had significantly lower Gb3 cell-surface expression recovery after 3 h or 5 h SIP incubations than that of WT HeLa cells (Fig. 3D). *SGPPI* KD cells similarly had significantly lower Gb3 cell-surface expression recovery after 1, 3, or 5 h SIP incubations than that of WT HeLa

cells (Fig. 3E). These data validate the genome-wide CRISPR/Cas9 KO screening results that *PLPP3* and *SGPPI* are positive regulators of SIP uptake and recycling into the Gb3 sphingolipid synthesis pathway.

We next examined the subcellular localization of *PLPP3* and *SGPPI* in WT HeLa cells by coexpressing either *SGPPI* or *PLPP3*, fused to eGFP, with red fluorescent protein-tagged organelle markers and analyzed the captured images for fluorescence colocalization using confocal fluorescence microscopy. *SGPPI* appeared localized to the ER, as its fluorescent signal highly overlapped with the ER marker fluorescent signal (Fig. 4A–E). In contrast, *PLPP3* highly colocalized with the plasma membrane marker fluorescent signal (Fig. 4F–J). These results show that *PLPP3* and *SGPPI* reside in distinct cellular compartments.

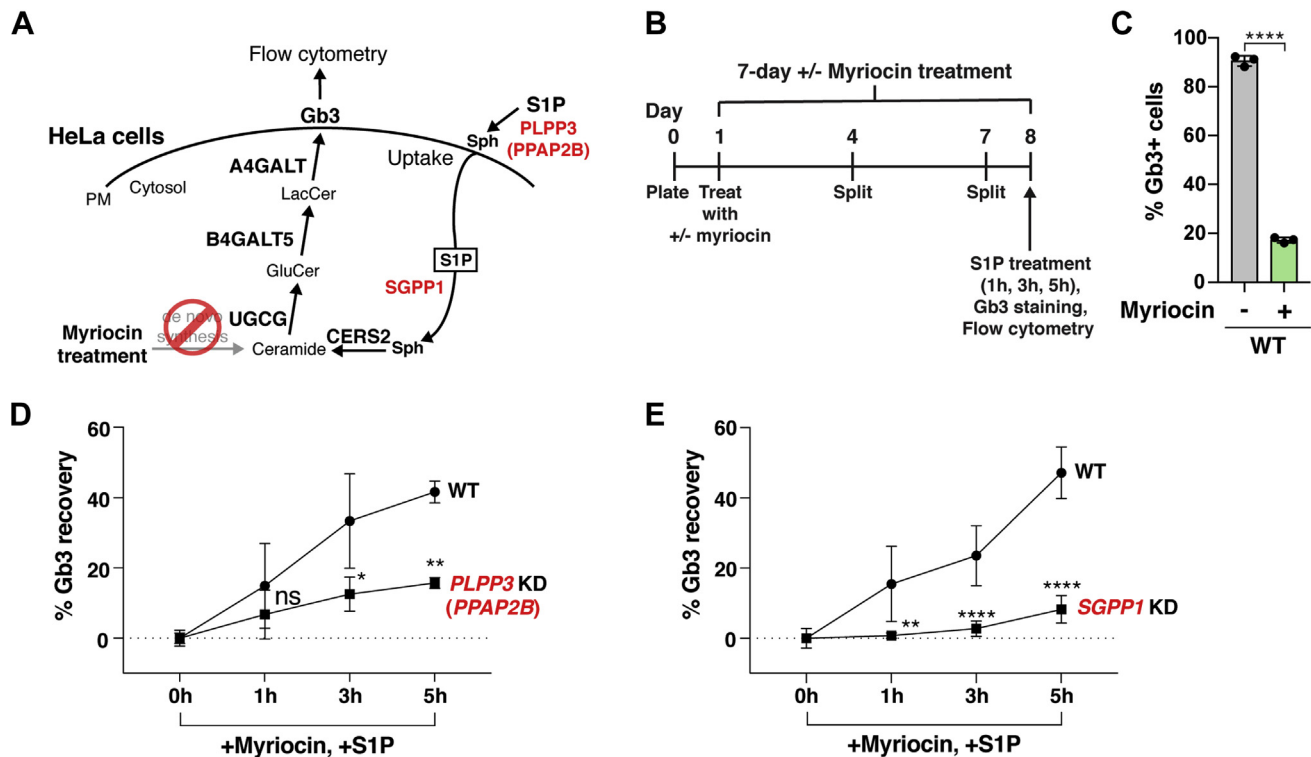


**Fig. 3.** *PLPP3* or *SGPP1* disruption reduces SIP-stimulated G<sub>b</sub>3 cell-surface expression. **A:** Schematic of the potential roles of *PLPP3* (*PPAP2B*) and *SGPP1* in the SIP uptake and recycling pathway. **B:** Timeline of experiment used to measure G<sub>b</sub>3 recovery after 2.5  $\mu$ M myriocin and 3  $\mu$ M SIP treatment in KD HeLa cells and WT HeLa cells. **C:** Validation of myriocin inhibition of de novo G<sub>b</sub>3 synthesis and subsequent cell-surface expression in WT HeLa cells. WT HeLa cells were cultured with 2.5  $\mu$ M myriocin for 7 days and cell-surface G<sub>b</sub>3 was measured by flow cytometry. Data represent the mean  $\pm$  SD (n = 3). **D:** G<sub>b</sub>3 cell-surface expression recovery rate after supplemental SIP treatment in myriocin-treated *PLPP3* KD HeLa cells and WT HeLa cells, based on flow cytometry. Experiments were performed twice using one *PLPP3* KD clone and WT HeLa cells (n = 6). **E:** G<sub>b</sub>3 cell-surface expression recovery rate after supplemental SIP treatment in myriocin-treated *SGPP1* KD HeLa cells and WT HeLa cells, based on flow cytometry. Experiments were performed three times using two *SGPP1* KD clones and WT HeLa cells (n = 9 for WT, n = 12 for *SGPP1*). **D** and **E:** G<sub>b</sub>3 cell-surface expression in the cells treated only with myriocin (0 h of SIP supplementation) was used as a baseline and subtracted from each data value. Experiments were conducted in triplicate wells for each condition. Data are presented as mean  $\pm$  SD. *P* values were determined by unpaired t-tests; \**P* < 0.05, \*\**P* < 0.01, \*\*\**P* < 0.0001. ns, not significant. G<sub>b</sub>3, globotriaosylceramide; KD, knockdown; PM, plasma membrane; Sph, sphingosine, SIP, sphingosine-1-phosphate.

### Sphingosine-kinase disruption enhances G<sub>b</sub>3 cell-surface expression

Sphingosine kinases should connect *PLPP3* and *SGPP1* in the recycling pathway by rephosphorylating the sphingosine product of *PLPP3* back to a SIP substrate available for *SGPP1* dephosphorylation (Fig. 5A). However, the sphingosine kinases, *SPHK1* and *SPHK2*, were not highly ranked in the genome-wide CRISPR/Cas9 KO screening we performed (i.e., they were not found in the top 100 positively ranked genes presented in supplemental Table S3). To investigate the role of sphingosine kinases in G<sub>b</sub>3 cell-surface expression, we created individual *SPHK1* KD and *SPHK2* KD, as well as *SPHK1/2* DKD, HeLa cells through Cas9-mediated gene disruption (supplemental Fig. S2C, D). In the absence of myriocin treatment, the *SPHK1* KD, *SPHK2* KD, and *SPHK1/2* DKD HeLa cells all displayed G<sub>b</sub>3 cell-surface expression comparable with that observed in WT HeLa cells (Fig. 5B, C). Extensive myriocin treatment to block de novo sphingolipid synthesis lowered G<sub>b</sub>3

cell-surface expression in WT HeLa cells by approximately 75%. The remaining fraction of G<sub>b</sub>3 cell-surface expression would presumably be due to salvage of sphingoid bases from residual sphingolipids in the cells and medium. Interestingly, the myriocin treatment was relatively ineffective in reducing G<sub>b</sub>3 cell-surface expression in cells deficient in *SPHKs* (Fig. 5C). When *SPHK1/2* DKD cells were treated with myriocin, G<sub>b</sub>3 expression was reduced by only approximately 10%. Exposure of myriocin-treated *SPHK1* KD, *SPHK2* KD, and *SPHK1/2* DKD HeLa cells to SIP significantly increased their G<sub>b</sub>3 cell-surface expression compared with what was observed in myriocin-treated cells without SIP exposure (Fig. 5B, C).

To ensure that the elevated G<sub>b</sub>3 cell-surface expression in the *SPHK* KD lines was not the result of ineffective inhibition of de novo sphingolipid synthesis by myriocin, we introduced a genetic block in the de novo sphingolipid synthesis pathway in the *SPHK1/2* DKD cells with the additional genetic disruption of

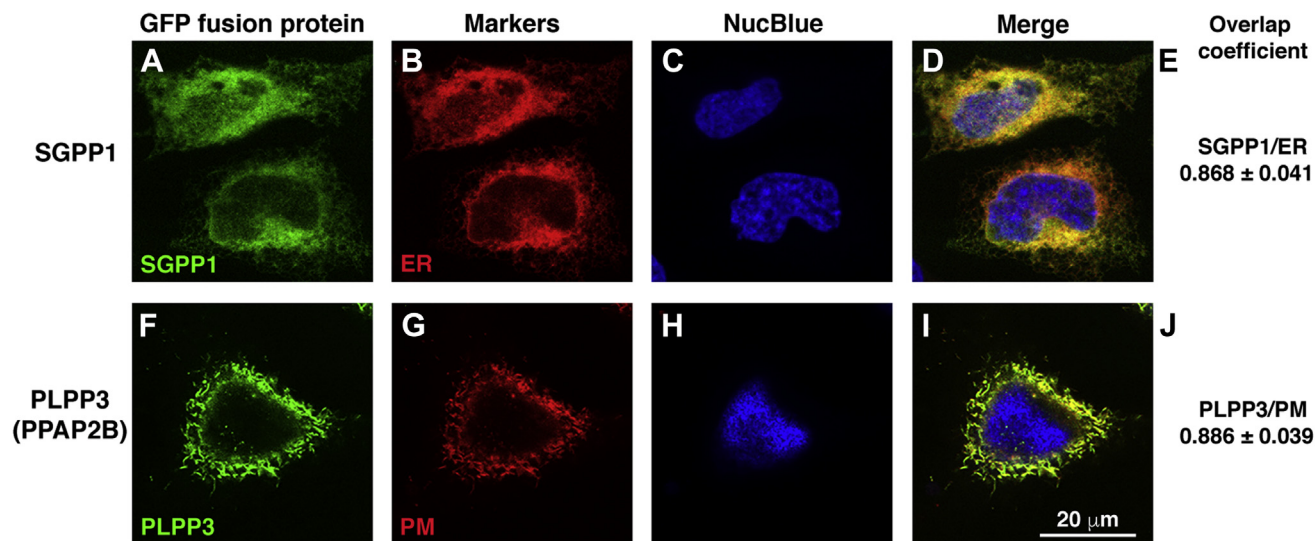


**Fig. 4.** SGPP1 localizes to the ER and PLPP3 (PPAP2B) localizes to the plasma membrane. A: *eGFP-SGPP1* and (F) *PLPP3 (PPAP2B)-eGFP* were transfected into HeLa cells along with RFP-tagged organelle markers (supplemental Table S1) for (B) ER and (G) plasma membrane (PM). C and H: Nuclei (blue) were stained by NucBlue Live Cell ReadyProbes Reagent (Hoechst 33,342). Cells were examined by confocal fluorescence microscopy. D and I: Merged images. E and J: Colocalization of fluorescent markers was determined by Manders overlap coefficient using ZEN Blue software (ZEN 2012 SP5). n=20–30 cells. RFP, red fluorescent protein.

*SPTLC1* to produce TKD cells (supplemental Fig. S2C–E). Even though the disruption of *SPTLC1* alone significantly reduced Gb3 cell-surface expression (Fig. 1B–D), when coupled to the disruption of both *SPHK* genes, significantly higher levels of Gb3 cell-surface expression were detected in myriocin-treated *SPHK1/SPHK2/SPTLC1* TKD cells than in myriocin-treated WT HeLa cells (Fig. 5D). Collectively, the results with pharmacologic and genetic blocks of de novo sphingolipid synthesis indicate that sphingosine-kinase disruption enhances sphingoid base salvage for recycling into the sphingolipid synthesis pathway. This finding provides an explanation for the absence of *SPHK1* and *SPHK2* as top hits in the genome-wide CRISPR/Cas9 KO screen, which was geared toward detecting genes that, when knocked out, depress the incorporation of sphingoid bases into the sphingolipid synthesis pathway.

Sphingosine-kinase disruption may enhance sphingoid base salvage, and Gb3 cell-surface expression, by eliminating the SIP degradation pathway mediated by SIP lyase (SGPL1) and thereby shunting sphingoid base substrate into the sphingolipid synthesis pathway (6, 29, 30). If so, the Gb3 cell-surface expression pattern of *SGPL1* KD HeLa cells should be similar to that of the *SPHK1/2* DKD cells (Fig. 5C). We produced validated *SGPL1* KD HeLa cells by Cas9-mediated gene disruption (supplemental Fig. S2F) and determined Gb3 cell-surface expression with and without treatment with myriocin to block de novo sphingolipid synthesis. In untreated *SGPL1* KD cells, Gb3 cell-surface expression was comparable with that observed in untreated WT HeLa cells. Myriocin treatment was relatively ineffective in reducing Gb3 cell-surface expression in *SGPL1*

KD cells compared to myriocin-treated WT HeLa cells (Fig. 5B, E), similar to what was observed for *SPHK1/2* DKD cells (Fig. 5C).

Lastly, we determined the subcellular localization of *SPHK1*, *SPHK2*, and *SGPL1* by coexpressing *eGFP*-tagged *SPHK1*, *SPHK2*, or *SGPL1* with organelle markers in WT HeLa cells and examining fluorescence colocalization. Similar to previous reports, *SPHK1* was found to be largely expressed in early endosomes (31) (Fig. 6A–E). *SPHK2* was expressed diffusely in the cytosol and nucleus (32, 33) (Fig. 6F–J). *SGPL1* localized to the ER (Fig. 6K–O) as has been described (34). These results confirm that the sphingosine kinases are broadly expressed on vesicles and in cytoplasmic and nuclear compartments and indicate that they are poised to convert sphingosine to SIP throughout the cell. *SGPL1*, along with *SGPP1*, is confined to the ER where they compete for SIP substrate.

## DISCUSSION

SIP is an extracellular-signaling sphingolipid whose metabolism regulates its signaling activity. It has two major intracellular metabolic fates (1–3): 1) degradation by SIP lyase and removal of sphingoid base substrate from the sphingolipid pathway or 2) salvage and recycling of its sphingoid base for sphingolipid synthesis. Recent studies have illuminated the pathway for the cellular uptake and SIP lyase-mediated degradation of extracellular SIP in hepatocytes (12). However, the pathway used for intracellular salvage of the sphingoid base from extracellular SIP and its recycling has not been clearly defined. We have used a genome-wide CRISPR/Cas9 KO screen to identify the genes

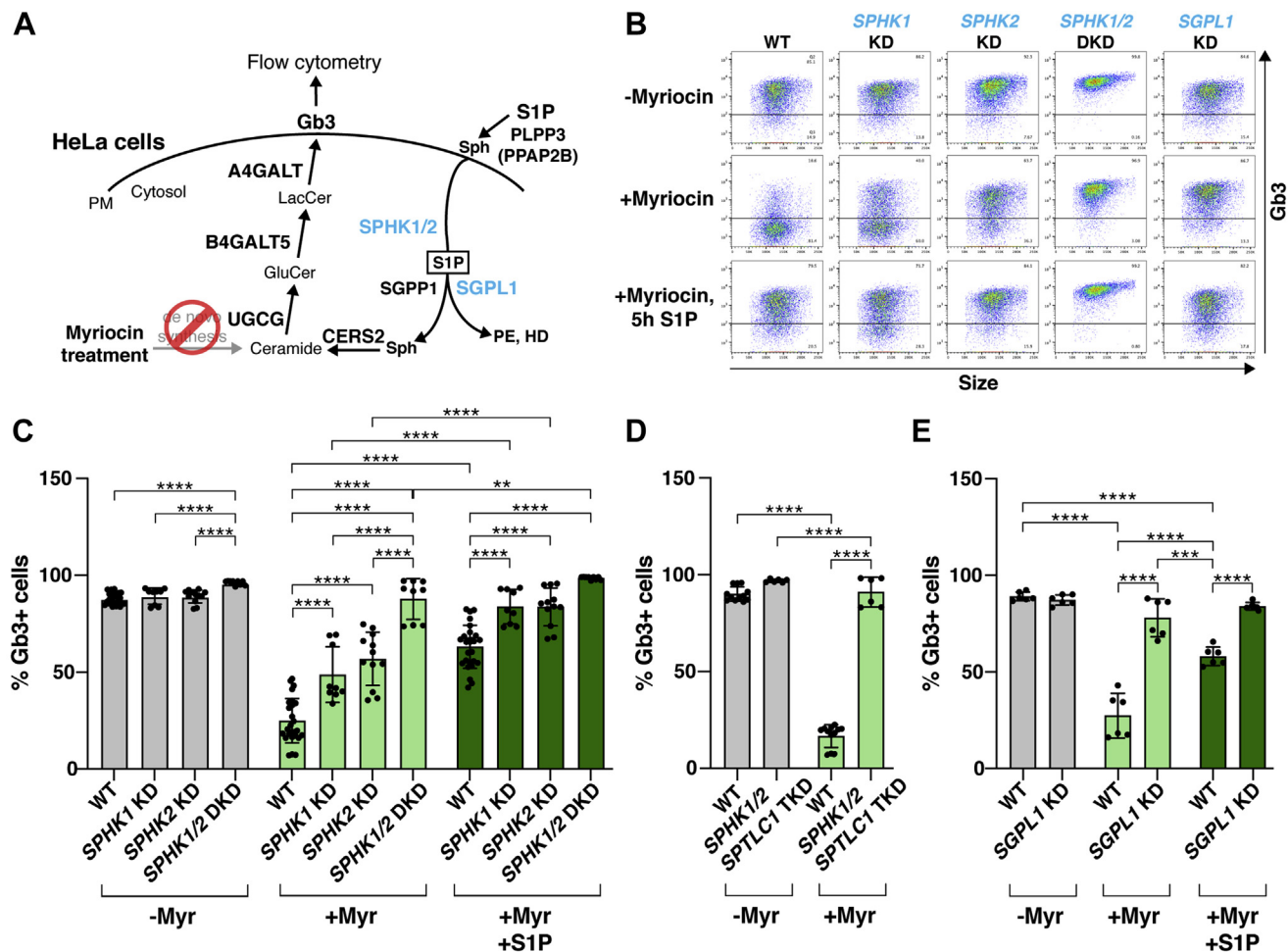


**Fig. 5.** *SPHK1*, *SPHK2*, or *SGPL1* KD elevates Gb3 cell-surface expression. **A:** Schematic of the potential roles of *SPHK1*, *SPHK2*, and *SGPL1* in the SIP recycling and degradation pathways. Myriocin treatment inhibits de novo Gb3 synthesis so that Gb3 synthesis via the recycling pathway can be analyzed. **B:** Representative dot plots of flow cytometry for WT, *SPHK1* KD, *SPHK2* KD, *SPHK1/2* DKD, and *SGPL1* KD HeLa cells under three different myriocin/SIP treatment conditions (no myriocin [7 days], 2.5  $\mu$ M myriocin [7 days], 2.5  $\mu$ M myriocin [7 days] followed by 3  $\mu$ M SIP [5 h]). **C, D, and E:** Quantification of Gb3 cell-surface expression based on flow cytometry data for cells that were not treated with myriocin (gray), treated with myriocin (light green), or treated with myriocin and SIP (dark green). **C:** Experiments were performed using the *SPHK1* KD cell pool, and two cell clones each for *SPHK2* KD and *SPHK1/2* DKD cells along with WT HeLa cells (WT, n = 24; *SPHK1* KD, n = 6; *SPHK2* KD, n = 12; *SPHK1/2* DKD, n = 9). **D:** Experiments were performed with two cell clones of *SPHK1/2/SPTLC1* TKD and WT HeLa cells (WT, n = 6; *SPHK1/2/SPTLC1* TKD, n = 6). **E:** Experiments were performed using the *SGPL1* KD cell pool and WT HeLa cells (WT, n = 6; *SGPL1* KD, n = 6). **C–E:** All experiments for each KD cell line were conducted in triplicate wells for each condition and repeated at least twice. Data represent the mean  $\pm$  SD. *P* values were determined by one-way ANOVA followed by Bonferroni's multiple comparisons test; \*\**P* < 0.01, \*\*\**P* < 0.001, \*\*\*\**P* < 0.0001. DKD, double knockdown; Gb3, globotriaosylceramide; HD, hexadecenal; KD, knockdown; PE, phosphoethanolamine; PM, plasma membrane; Sph, sphingosine; SIP, sphingosine-1-phosphate; TKD, triple knockdown.

responsible for this SIP cellular uptake and sphingoid base salvage for recycling into the sphingolipid synthesis pathway.

Among the genes we identified for uptake sphingoid base salvage and recycling were two distinct lipid phosphatases, *PLPP3* and *SGPP1*. Also known as LPP3, PAP-2b, or PPAP2B, *PLPP3* is an integral-membrane protein with an extracellular-facing active site that catalyzes the dephosphorylation of a variety of lipid phosphates, including SIP (35–38). We found that *PLPP3* was exclusively expressed at the plasma membrane in WT HeLa cells, which was in agreement with previous studies (39–41). At the hepatocyte surface,

*PLPP3* has been shown to dephosphorylate blood SIP, allowing sphingosine to enter hepatocytes for rephosphorylation by *Sphk2* and subsequent degradation by SIP lyase (12). Similarly, in human myeloid-derived HAP1 cells, the three-member PLPP family, including *PLPP3*, was demonstrated to be important for the efficient handling of exogenous SIP, although some *PLPP*-independent uptake was also detected (42). In human lung endothelial cells, *PLPP1* was found to stimulate uptake of the sphingoid base of SIP, which was then subjected to rephosphorylation by *SPHK1* (43). Interestingly, adipocyte *PLPP3* deficiency was found to regulate sphingolipid synthesis, resulting in reduced



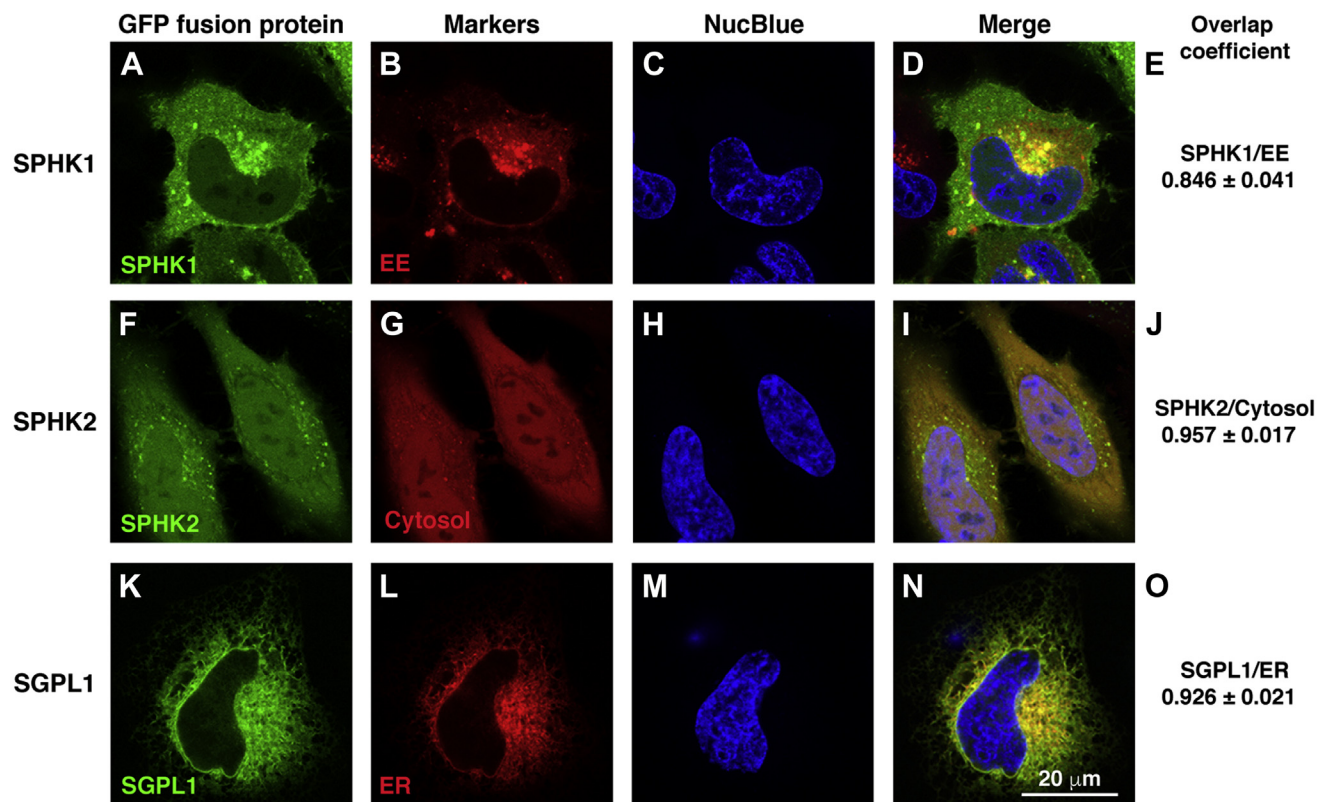


**Fig. 6.** SPHK1 localizes to the early endosomes, SPHK2 localizes to the cytosol and nucleus, and SGPL1 localizes to the ER. A: *eGFP-SPHK1*, (F) *eGFP-SPHK2*, and (K) *SGPL1-eGFP* were transfected into HeLa cells along with RFP-tagged organelle markers (supplemental Table S1) for (B) early endosomes (EE) or (L) ER, or with mCherry2-C1 plasmid for (G) cytosol. C, H, and M: Nuclei (blue) were stained by NucBlue Live Cell Stain ReadyProbeReagent (Hoechst 33342). Cells were examined by confocal fluorescence microscopy. D, I, and N: Merged images. E, J, and O: Colocalization of fluorescent markers was determined by Manders overlap coefficient using ZEN Blue software (ZEN 2012 SP5). n=20–30 cells. RFP, red fluorescent protein.

ceramide and sphingomyelin accumulation during adipose-tissue expansion (44). The other two PLPP family members, although expressed in HeLa cells (Human Protein Atlas [proteintatlas.org](http://proteintatlas.org)), were not detected in the screen indicating that PLPP3 is dominant in initiating SIP uptake by dephosphorylation of exogenous SIP.

SGPPI is a lipid phosphatase that specifically catalyzes dephosphorylation of SIP (45). We found that SGPPI localized to the ER in HeLa cells, which is consistent with previous findings that SGPPI and its homologs in yeast (46), mouse (47), and human (48) are ER integral-membrane proteins. Overexpression of SGPPI has been shown to stimulate the incorporation of sphingosine into ceramide for the production of glycosphingolipids (49). SGPP2, while structurally and functionally similar to SGPPI (50), is not well expressed in HeLa cells possibly explaining its absence among the hits in the screen (Human Protein Atlas [proteintatlas.org](http://proteintatlas.org)).

The different locations of PLPP3 and SGPPI imply that extracellular SIP is dephosphorylated in two disparate subcellular compartments during a dephosphorylation-phosphorylation-dephosphorylation cycle prior to the incorporation of its sphingoid base into the sphingolipid

synthesis pathway. In this scheme, the sphingosine product of PLPP3 generated at the plasma membrane would be rephosphorylated in the cytoplasm by the sphingosine kinases. The newly formed intracellular SIP would then be transferred to the ER surface, by a yet to-be-explained process, where it would be dephosphorylated by SGPPI to generate sphingoid base substrate for ceramide production (Fig. 7). Other top hits in the screen included core biosynthetic enzymes responsible for Gb3 production (CERS2, UGCG, B4GALT5, A4GALT), proteins that support glycosphingolipid synthesis in the Golgi (LAPTM4A, TM9SF2, SLC35A2, TMEM165, GOLPH3), and a transcription factor (AHR) that regulates glycosphingolipid synthesis gene expression (Fig. 7).

In yeast, previous studies have indicated that exogenous sphingoid bases undergo a cycle of phosphorylation and dephosphorylation to be efficiently incorporated into ceramides and sphingolipids (51–54). Although this cycle can be bypassed, sphingolipids are synthesized less efficiently if exogenous sphingoid bases cannot be phosphorylated (51–54).

Our findings indicate that, in HeLa cells, the sphingosine kinases do not appear to be needed for Gb3 synthesis via the salvage of sphingoid base from extracellular SIP and its recycling into the sphingolipid

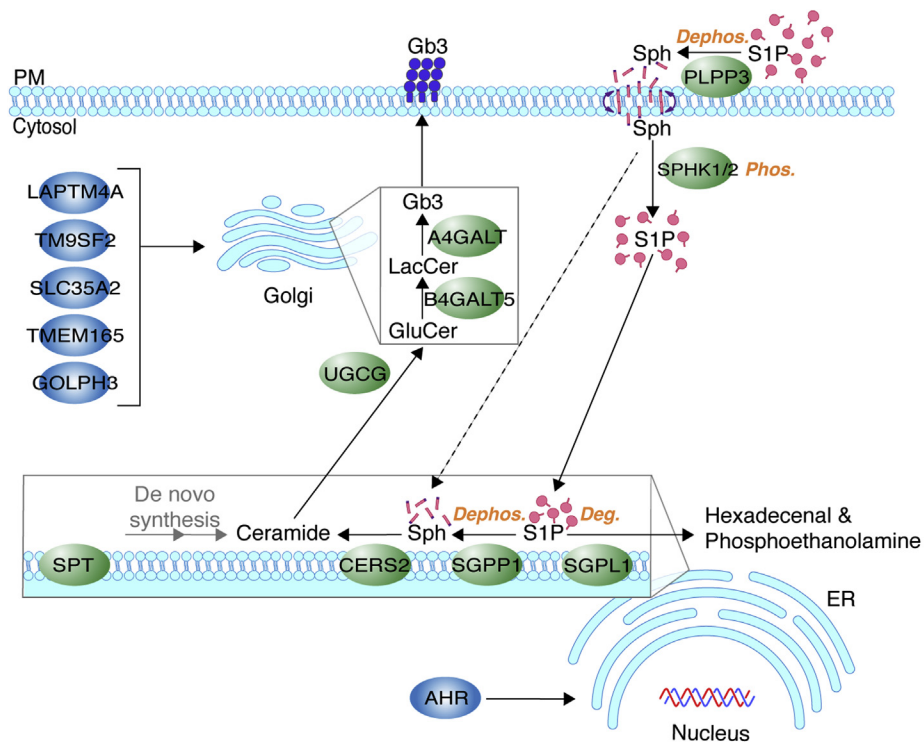


**Fig. 7.** Proposed pathway for SIP cellular uptake and incorporation into the sphingolipid synthesis pathway. Plasma membrane-resident PLPP3 dephosphorylates exogenous SIP to sphingosine, which enters cells by a flip-flop mechanism and is phosphorylated to SIP by SPHKs 1 and 2. Intracellular SIP serves as a branch-point substrate for ER-resident SGPP1 and SGPL1. SGPP1 dephosphorylates SIP to sphingosine, which is utilized for ceramide synthesis (CERS2) and sequential modifications for glycosphingolipid production. SGPL1 irreversibly degrades SIP to hexadecenal and phosphoethanolamine, allowing exit of the substrate from the sphingolipid synthesis pathway. These enzymes work in concert to drive an SIP dephosphorylation-phosphorylation-dephosphorylation/degradation cycle. In the absence of sphingosine kinases, sphingosine may bypass the cycle and directly serve as a CERS2 substrate (dashed line), thereby being excluded from the SGPL1-mediated degradation pathway. UGCG, B4GALT5, and A4GALT are Golgi core glycosphingolipid synthesis enzymes for synthesis of Gb3. LAPT4A, TM9SF2, SLC35A2, TMEM165, and GOLPH3 are positive regulators of Gb3 synthesis in the Golgi. AHR is a transcriptional activator of genes involved in glycosphingolipid synthesis. Deg, degradation; Dephos, dephosphorylation; Gb3, globotriaosylceramide; Phos, phosphorylation; PM, plasma membrane; Sph, sphingosine; S1P, sphingosine-1-phosphate


synthesis pathway. First, our genome-wide CRISPR/Cas9 KO screen identified both phosphatases as positive regulators of sphingoid base recycling into the Gb3 synthesis pathway but did not pick up the sphingosine kinases as regulators of this process. Second, knocking down sphingosine-kinase expression in cells with the de novo sphingolipid synthesis pathway disabled led to elevated Gb3 cell-surface expression, apparently due to enhanced salvage of sphingoid bases for use in sphingolipid synthesis. The enhanced Gb3 cell-surface expression in cells deficient in sphingosine kinase may be due to the inability to produce a substrate for SIP lyase, effectively blocking the degradation pathway and thus salvaging sphingoid bases for incorporation into new sphingolipids (Fig. 7, dashed-line arrow). Indeed, we found a similar enhancement of Gb3 cell-surface expression when SIP lyase was knocked down in HeLa cells. Other studies have also confirmed that disruption of SIP lyase activity stimulates sphingoid base salvage and recycling (55, 56).

SIP, when in circulation, is predominately bound to carrier proteins, HDL, and serum albumin (4). In our screen, SIP was added to HeLa cells without carrier proteins, a form

that was taken up as well as carrier-bound SIP. However, under these conditions, we may not have identified cell surface receptors involved in the uptake of carrier-bound SIP for subsequent entry into the recycling pathway.

The dephosphorylation-phosphorylation-dephosphorylation cycle for extracellular SIP provides several key functions. The dephosphorylation of extracellular SIP controls its extracellular levels by allowing lipid uptake into cells. The sphingoid base liberated by PLPP3 may pass through the plasma membrane by a flip-flop mechanism as proposed for hepatocytes (12) (Fig. 7). The subsequent sphingosine kinase-mediated rephosphorylation of sphingoid bases entering cells prevents severe disturbances in endocytic trafficking and autophagic function (31, 57, 58). This rephosphorylation step also serves to produce a critical branch-point substrate (59, 60), SIP, allowing either sphingoid base removal from the sphingolipid synthesis pathway via degradation by SIP lyase or its preservation in the pathway by the second SIP dephosphorylation step in the ER for sphingoid base salvage and subsequent recycling, a concerted process that is critical for the control of sphingolipid levels (49, 55).

## Data availability

All data are included in the article and supporting information. 

## Supplemental data

This article includes supplemental data.

## Acknowledgments

We thank Linda Raab for editing and suggestions for improving the article. This work was supported by the Intramural Research Program of the National Institutes of Health, National Institute of Diabetes and Digestive and Kidney Diseases, USA.

## Author contributions

M. K., L. H.-H., S. M., R. S., C. B., H. Z., and R. L. P. conceptualization; M. K., L. H.-H., S. M., R. S., C. B., and H. Z. investigation; M. K., L. H.-H., S. M., R. S., C. B., H. Z., and R. L. P. formal analysis; M. K., L. H.-H., and R. L. P. writing—original draft; M. K., L. H.-H., S. M., R. S., C. B., H. Z., and R. L. P. Writing—review and editing.

## Author ORCIDs

Mari Kono  <https://orcid.org/0000-0003-2447-4350>

Lila E. Hoachlander-Hobby  <https://orcid.org/0000-0003-3054-9048>

Saurav Majumder  <https://orcid.org/0000-0002-5067-1190>

Ronit Schwartz  <https://orcid.org/0000-0003-4297-3495>

Hongling Zhu  <https://orcid.org/0000-0003-0612-009X>

Richard L. Proia  <https://orcid.org/0000-0003-0456-1270>

## Funding and additional information

The content is solely the responsibility of the authors and does not necessarily represent the official views of the National Institutes of Health.

## Conflict of interest

The authors declare no competing interests.

## Abbreviations

CRISPR, clustered regularly interspersed short palindromic repeats; DKD, double knockdown; Gb3, globotriaosylceramide; GeCKO, genome-wide CRISPR/Cas9 KO; KD, knockdown; MAGeCK, model-based analysis of genome-wide CRISPR-Cas9 KO; MOI, multiplicity of infection; SIP, sphingosine-1-phosphate; sgRNA, single guide RNA; TKD, triple knockdown.

Manuscript received January 6, 2022, and in revised form May 6, 2022. Published, JLR Papers in Press, May 11, 2022, <https://doi.org/10.1016/j.jlr.2022.100225>

## REFERENCES

- Merrill, A. H., Jr. (2011) Sphingolipid and glycosphingolipid metabolic pathways in the era of sphingolipidomics. *Chem. Rev.* **111**, 6387–6422
- Hannun, Y. A., and Obeid, L. M. (2018) Sphingolipids and their metabolism in physiology and disease. *Nat. Rev. Mol. Cell Biol.* **19**, 175–191
- Sandhoff, R., Schulze, H., and Sandhoff, K. (2018) Ganglioside Metabolism in Health and Disease. *Prog. Mol. Biol. Transl. Sci.* **156**, 1–62
- Proia, R. L., and Hla, T. (2015) Emerging biology of sphingosine-1-phosphate: its role in pathogenesis and therapy. *J. Clin. Invest.* **125**, 1379–1387
- Green, C. D., Maceyka, M., Cowart, L. A., and Spiegel, S. (2021) Sphingolipids in metabolic disease: the good, the bad, and the unknown. *Cell Metab.* **33**, 1293–1306
- Saba, J. D. (2019) Fifty years of lyase and a moment of truth: sphingosine phosphate lyase from discovery to disease. *J. Lipid Res.* **60**, 456–463
- Olivera, A., Allende, M. L., and Proia, R. L. (2013) Shaping the landscape: metabolic regulation of SIP gradients. *Biochim. Biophys. Acta.* **1831**, 193–202
- Baeyens, A. A. L., and Schwab, S. R. (2020) Finding a way out: SIP signaling and immune cell migration. *Annu. Rev. Immunol.* **38**, 759–784
- Peest, U., Sensken, S. C., Andreani, P., Hanel, P., Van Veldhoven, P. P., and Graler, M. H. (2008) SIP-lyase independent clearance of extracellular sphingosine 1-phosphate after dephosphorylation and cellular uptake. *J. Cell Biochem.* **104**, 756–772
- Venkataraman, K., Lee, Y. M., Michaud, J., Thangada, S., Ai, Y., Bonkovsky, H. L., et al. (2008) Vascular endothelium as a contributor of plasma sphingosine 1-phosphate. *Circ. Res.* **102**, 669–676
- Salous, A. K., Panchatcharam, M., Sunkara, M., Mueller, P., Dong, A., Wang, Y., et al. (2013) Mechanism of rapid elimination of lysophosphatidic acid and related lipids from the circulation of mice. *J. Lipid Res.* **54**, 2775–2784
- Kharel, Y., Huang, T., Salamon, A., Harris, T. E., Santos, W. L., and Lynch, K. R. (2020) Mechanism of sphingosine 1-phosphate clearance from blood. *Biochem. J.* **477**, 925–935
- Sanjana, N. E., Shalem, O., and Zhang, F. (2014) Improved vectors and genome-wide libraries for CRISPR screening. *Nat. Met.* **11**, 783–784
- Li, W., Xu, H., Xiao, T., Cong, L., Love, M. I., Zhang, F., et al. (2014) MAGeCK enables robust identification of essential genes from genome-scale CRISPR/Cas9 knockout screens. *Genome Biol.* **15**, 554
- Sattler, K., Graler, M., Keul, P., Weske, S., Reimann, C. M., Jindrova, H., et al. (2015) Defects of high-density lipoproteins in coronary artery disease caused by low sphingosine-1-phosphate content: correction by sphingosine-1-phosphate-loading. *J. Am. Coll. Cardiol.* **66**, 1470–1485
- Lee, M. J., Van Brocklyn, J. R., Thangada, S., Liu, C. H., Hand, A. R., Menzeleev, R., et al. (1998) Sphingosine-1-phosphate as a ligand for the G protein-coupled receptor EDG-1. *Science* **279**, 1552–1555
- Jacewicz, M., Clausen, H., Nudelman, E., Donohue-Rolfe, A., and Keusch, G. T. (1986) Pathogenesis of shigella diarrhea. XI. Isolation of a shigella toxin-binding glycolipid from rabbit jejunum and HeLa cells and its identification as globotriaosylceramide. *J. Exp. Med.* **163**, 1391–1404
- Keusch, G. T., Jacewicz, M., Acheson, D. W., Donohue-Rolfe, A., Kane, A. V., and McCluer, R. H. (1995) Globotriaosylceramide, Gb3, is an alternative functional receptor for Shiga-like toxin 2e. *Infect. Immun.* **63**, 1138–1141
- Lindberg, A. A., Brown, J. E., Stromberg, N., Westling-Ryd, M., Schultz, J. E., and Karlsson, K. A. (1987) Identification of the carbohydrate receptor for Shiga toxin produced by *Shigella dysenteriae* type 1. *J. Biol. Chem.* **262**, 1779–1785
- Majumder, S., Kono, M., Lee, Y. T., Byrnes, C., Li, C., Tuymetova, G., et al. (2020) A genome-wide CRISPR/Cas9 screen reveals that the aryl hydrocarbon receptor stimulates sphingolipid levels. *J. Biol. Chem.* **295**, 4341–4349
- Tian, S., Muneeruddin, K., Choi, M. Y., Tao, L., Bhuiyan, R. H., Ohmi, Y., et al. (2018) Genome-wide CRISPR screens for Shiga toxins and ricin reveal Golgi proteins critical for glycosylation. *PLoS Biol.* **16**, e2006951
- Yamaji, T., Sekizuka, T., Tachida, Y., Sakuma, C., Morimoto, K., Kuroda, M., et al. (2019) A CRISPR screen identifies LAPTMA4 and TM9SF proteins as glycolipid-regulating factors. *iScience* **11**, 409–424
- Pacheco, A. R., Lazarus, J. E., Sit, B., Schmieder, S., Lencer, W. I., Blondel, C. J., et al. (2018) CRISPR screen reveals that EHEC's T3SS and Shiga toxin rely on shared host factors for infection. *mBio* **9**, e01003-18
- Witters, P., Tahata, S., Barone, R., Ounap, K., Salvarinova, R., Gronborg, S., et al. (2020) Clinical and biochemical improvement with galactose supplementation in SLC35A2-CDG. *Genet. Med.* **22**, 1102–1107

25. Yates, T. M., Suri, M., Desurkar, A., Lesca, G., Wallgren-Pettersson, C., Hammer, T. B., *et al.* (2018) SLC35A2-related congenital disorder of glycosylation: defining the phenotype. *Eur. J. Paediatr. Neurol.* **22**, 1095–1102
26. Potelle, S., Morelle, W., Dulary, E., Duvet, S., Vicogne, D., Spriet, C., *et al.* (2016) Glycosylation abnormalities in Gdt1p/TMEM165 deficient cells result from a defect in Golgi manganese homeostasis. *Hum. Mol. Genet.* **25**, 1489–1500
27. Stribny, J., Thines, L., Deschamps, A., Goffin, P., and Morsomme, P. (2020) The human Golgi protein TMEM165 transports calcium and manganese in yeast and bacterial cells. *J. Biol. Chem.* **295**, 3865–3874
28. Rizzo, R., Russo, D., Kurokawa, K., Sahu, P., Lombardi, B., Supino, D., *et al.* (2021) Golgi maturation-dependent glycoenzyme recycling controls glycosphingolipid biosynthesis and cell growth via GOLPH3. *EMBO J.* **40**, e107238
29. Kihara, A. (2014) Sphingosine 1-phosphate is a key metabolite linking sphingolipids to glycerophospholipids. *Biochim. Biophys. Acta.* **1841**, 766–772
30. Maceyka, M., Harikumar, K. B., Milstien, S., and Spiegel, S. (2012) Sphingosine-1-phosphate signaling and its role in disease. *Trends Cell Biol.* **22**, 50–60
31. Shen, H., Giordano, F., Wu, Y., Chan, J., Zhu, C., Milosevic, I., *et al.* (2014) Coupling between endocytosis and sphingosine kinase 1 recruitment. *Nat. Cell Biol.* **16**, 652–662
32. Hait, N. C., Allegood, J., Maceyka, M., Strub, G. M., Harikumar, K. B., Singh, S. K., *et al.* (2009) Regulation of histone acetylation in the nucleus by sphingosine-1-phosphate. *Science* **325**, 1254–1257
33. Igarashi, N., Okada, T., Hayashi, S., Fujita, T., Jahangeer, S., and Nakamura, S. (2003) Sphingosine kinase 2 is a nuclear protein and inhibits DNA synthesis. *J. Biol. Chem.* **278**, 46832–46839
34. Ikeda, M., Kihara, A., and Igarashi, Y. (2004) Sphingosine-1-phosphate lyase SPL is an endoplasmic reticulum-resident, integral membrane protein with the pyridoxal 5'-phosphate binding domain exposed to the cytosol. *Biochem. Biophys. Res. Commun.* **325**, 338–343
35. Hooks, S. B., Ragan, S. P., and Lynch, K. R. (1998) Identification of a novel human phosphatidic acid phosphatase type 2 isoform. *FEBS Lett.* **427**, 188–192
36. Jamal, Z., Martin, A., Gomez-Munoz, A., and Brindley, D. N. (1991) Plasma membrane fractions from rat liver contain a phosphatidate phosphohydrolase distinct from that in the endoplasmic reticulum and cytosol. *J. Biol. Chem.* **266**, 2988–2996
37. Kai, M., Wada, I., Imai, S., Sakane, F., and Kanoh, H. (1997) Cloning and characterization of two human isozymes of Mg<sup>2+</sup>-independent phosphatidic acid phosphatase. *J. Biol. Chem.* **272**, 24572–24578
38. Roberts, R., Sciorra, V. A., and Morris, A. J. (1998) Human type 2 phosphatidic acid phosphohydrolases. Substrate specificity of the type 2a, 2b, and 2c enzymes and cell surface activity of the 2a isoform. *J. Biol. Chem.* **273**, 22059–22067
39. Ishikawa, T., Kai, M., Wada, I., and Kanoh, H. (2000) Cell surface activities of the human type 2b phosphatidic acid phosphatase. *J. Biochem.* **127**, 645–651
40. Kai, M., Wada, I., Imai, S., Sakane, F., and Kanoh, H. (1996) Identification and cDNA cloning of 35-kDa phosphatidic acid phosphatase (type 2) bound to plasma membranes. Polymerase chain reaction amplification of mouse H<sub>2</sub>O<sub>2</sub>-inducible hic53 clone yielded the cDNA encoding phosphatidic acid phosphatase. *J. Biol. Chem.* **271**, 18931–18938
41. Sciorra, V. A., and Morris, A. J. (1999) Sequential actions of phospholipase D and phosphatidic acid phosphohydrolase 2b generate diglyceride in mammalian cells. *Mol. Biol. Cell* **10**, 3863–3876
42. Goto, H., Miyamoto, M., and Kihara, A. (2021) Direct uptake of sphingosine-1-phosphate independent of phospholipid phosphatases. *J. Biol. Chem.* **296**, 100605
43. Zhao, Y., Kalari, S. K., Usatyuk, P. V., Gorshkova, I., He, D., Watkins, T., *et al.* (2007) Intracellular generation of sphingosine 1-phosphate in human lung endothelial cells: role of lipid phosphate phosphatase-1 and sphingosine kinase 1. *J. Biol. Chem.* **282**, 14165–14177
44. Federico, L., Yang, L., Brandon, J., Panchatcharam, M., Ren, H., Mueller, P., *et al.* (2018) Lipid phosphate phosphatase 3 regulates adipocyte sphingolipid synthesis, but not developmental adipogenesis or diet-induced obesity in mice. *PLoS One.* **13**, e0198063
45. Mandala, S. M. (2001) Sphingosine-1-phosphate phosphatases. *Prostaglandins Other Lipid Mediat.* **64**, 143–156
46. Mao, C., Saba, J. D., and Obeid, L. M. (1999) The dihydro-sphingosine-1-phosphate phosphatases of *Saccharomyces cerevisiae* are important regulators of cell proliferation and heat stress responses. *Biochem. J.* **342**, 667–675
47. Le Stunff, H., Peterson, C., Thornton, R., Milstien, S., Mandala, S. M., and Spiegel, S. (2002) Characterization of murine sphingosine-1-phosphate phosphohydrolase. *J. Biol. Chem.* **277**, 8920–8927
48. Johnson, K. R., Johnson, K. Y., Becker, K. P., Bielawski, J., Mao, C., and Obeid, L. M. (2003) Role of human sphingosine-1-phosphate phosphatase 1 in the regulation of intra- and extracellular sphingosine-1-phosphate levels and cell viability. *J. Biol. Chem.* **278**, 34541–34547
49. Le Stunff, H., Giussani, P., Maceyka, M., Lepine, S., Milstien, S., and Spiegel, S. (2007) Recycling of sphingosine is regulated by the concerted actions of sphingosine-1-phosphate phosphohydrolase 1 and sphingosine kinase 2. *J. Biol. Chem.* **282**, 34372–34380
50. Ogawa, C., Kihara, A., Gokoh, M., and Igarashi, Y. (2003) Identification and characterization of a novel human sphingosine-1-phosphate phosphohydrolase, hSPP2. *J. Biol. Chem.* **278**, 1268–1272
51. Qie, L., Nagiec, M. M., Baltisberger, J. A., Lester, R. L., and Dickson, R. C. (1997) Identification of a *Saccharomyces* gene, LCB3, necessary for incorporation of exogenous long chain bases into sphingolipids. *J. Biol. Chem.* **272**, 16110–16117
52. Mao, C., Wadleigh, M., Jenkins, G. M., Hannun, Y. A., and Obeid, L. M. (1997) Identification and characterization of *Saccharomyces cerevisiae* dihydro-sphingosine-1-phosphate phosphatase. *J. Biol. Chem.* **272**, 28690–28694
53. Mandala, S. M., Thornton, R., Tu, Z., Kurtz, M. B., Nickels, J., Broach, J., *et al.* (1998) Sphingosine base 1-phosphate phosphatase: a key regulator of sphingolipid metabolism and stress response. *Proc. Natl. Acad. Sci. U. S. A.* **95**, 150–155
54. Funato, K., Lombardi, R., Vallee, B., and Riezman, H. (2003) Lcb4p is a key regulator of ceramide synthesis from exogenous long chain sphingoid base in *Saccharomyces cerevisiae*. *J. Biol. Chem.* **278**, 7325–7334
55. Bektas, M., Allende, M. L., Lee, B. G., Chen, W., Amar, M. J., Remaley, A. T., *et al.* (2010) Sphingosine 1-phosphate lyase deficiency disrupts lipid homeostasis in liver. *J. Biol. Chem.* **285**, 10880–10889
56. Hagen-Euteneuer, N., Lutjohann, D., Park, H., Merrill, A. H., Jr., and van Echten-Deckert, G. (2012) Sphingosine 1-phosphate (SIP) lyase deficiency increases sphingolipid formation via recycling at the expense of de novo biosynthesis in neurons. *J. Biol. Chem.* **287**, 9128–9136
57. Young, M. M., Takahashi, Y., Fox, T. E., Yun, J. K., Kester, M., and Wang, H. G. (2016) Sphingosine kinase 1 cooperates with autophagy to maintain endocytic membrane trafficking. *Cell Rep.* **17**, 1532–1545
58. Lima, S., Milstien, S., and Spiegel, S. (2017) Sphingosine and Sphingosine Kinase 1 Involvement in Endocytic Membrane Trafficking. *J. Biol. Chem.* **292**, 3074–3088
59. Perez Rafael, S., Vallee-Belisle, A., Fabregas, E., Plaxco, K., Pallechi, G., and Ricci, F. (2012) Employing the metabolic "branch point effect" to generate an all-or-none, digital-like response in enzymatic outputs and enzyme-based sensors. *Anal. Chem.* **84**, 1076–1082
60. LaPorte, D. C., Walsh, K., and Koshland, D. E., Jr. (1984) The branch point effect. Ultrasensitivity and subsensitivity to metabolic control. *J. Biol. Chem.* **259**, 14068–14075